

## Effect of firing temperatures on alkali activated Geopolymer mortar doped with MWCNT

H.M. Khater\* and H.A. Abd El Gawwad<sup>a</sup>

Housing and Building National Research Centre (HBNRC), 87 El-Tahreer St., Dokki, Giza,  
P.O. Box 1770, Cairo, Egypt

(Received July 8, 2015, Revised December 25, 2015, Accepted December 29, 2015)

**Abstract.** The current investigation aims to study performance of geopolymer mortar reinforced with Multiwalled carbon nanotubes upon exposure to 200°C to 1000°C for 2 hrs. MWCNTs are doped into slag Geopolymer mortar matrices in the ratio of 0.0 to 0.4, % by weight of binder. Mortar composed of calcium aluminosilicate to sand (1:2), however, binder composed of 50% air cooled slag and 50% water cooled slag. Various water / binder ratios in the range of 0.114-0.129 used depending on the added MWCNT, while 6 wt., % sodium hydroxide used as an alkali activator. Results illustrate reduction in mechanical strength with temperature except specimens containing 0.1 and 0.2% MWCNT at 200°C, while further increase in temperature leads to decrease in strength values of the resulting geopolymer mortar. Also, decrease in firing shrinkage with MWCNT up to 0.1% at all firing temperatures up to 500°C is observed, however the shrinkage values increase with temperature up to 500°C. Further increase on the firing temperature up to 1000°C results in an increase in the volume due to expansion.

**Keywords:** MWCNT; geopolymer; mortar; WCS; ACS; thermal stability

---

### 1. Introduction

Makar *et al.* (2005) stated that the composites containing carbon Nano-tubes considered being of better mechanical and thermal properties as ideal reinforcing materials. There are many different morphological shapes of CNTs as single or multiple wall sheets rolled up in a tube or a series of tubes. The unique graphene structure endows CNTs with extraordinary characteristics, where their density are less than that of steel or glass fiber, also CNTs have an elastic modulus in the terapascal range, yield strength of approximately 20-60 GPa, and yield strain of up to 10 %, far surpassing traditional carbon fibers in these regards (Walters 1999). Moreover, due to their remarkable mechanical, electrical, thermal properties, excellent Nano scale effects, low density, and excellent chemical and thermal stability; nano carbon materials (NCMs) offer a new generation of high-performance,, and multifunctional cementitious composites (Sanchez and Sobolev 2010, Raki *et al.* 2010, Sobolev and Gutiérrez 2005, Mukhopadhyay 2011). Many researchers demon strated the potential of various NCMs including carbon nanofibres (CNFs),

---

\*Corresponding author, Associate Professor, E-mail: Hkhater4@yahoo.com

<sup>a</sup>Researcher

carbon nanotubes (CNTs) and nano graphite platelets (NGPs) for enhancing/ modifying cementitious materials (Parveen *et al.* 2013, Li *et al.* 2005, Gao and Mo 2009, Huang 2012, Han *et al.* 2011, Han *et al.* 2013). Li *et al.* (2005) observed that addition of 0.5 wt. % CNTs can improve the flexural, compressive strength and the failure strain of the composites by 25%, 19% and 27%, respectively. Raki *et al.* (2010) stated that CNTs can improve the hardness of the early hydration of composites by 600%, Young modulus by 227% and the flexural strength by 40%. Gao and Mo (2009) (9) reported that compressive strength of composites with 0.16 wt. % CNFs is 42.7% higher than that of the plain cementitious materials. Huang (2012) obtained a maximum increase of 82% in flexural strength by adding NGPs into cementitious materials. NCMs achieve the enhancement effect by nucleation, increasing the amount of C-S-H gel of high hardness, improving pore structures, controlling Nanoscale cracks, improving the early strain capacity and reducing autogenous shrinkage of cementitious composites (Raki *et al.* 2010, Sobolev and Gutiérrez 2005, Mukhopadhyay 2011, Parveen *et al.* 2013, Li *et al.* 2005, Gao and Mo 2009, Huang 2012, Han *et al.* 2011, Han *et al.* 2013). In addition, due to their excellent electrical, thermal and electromagnetic properties, NCMs can improve electrical, thermal, electromagnetic and sensing properties to cementitious materials. Research efforts have been directed toward the development of cementitious composites with NCMs, and many innovative achievements have been gained in both development and application of the NCMs filled cementitious composites (NFCC); with strong potential applicability in numerous engineering fields (Fakhru'l-Razi *et al.* 2006, Khalili and Haghbin 2013, Laurenzi *et al.* 2013, Bi *et al.* 2013, Uddin *et al.* 2010).

In the field of construction, polymer composites are lower usages as compared with cement composites including concrete, mortar, and cement paste as structural and non-structural elements due to their mechanical properties, incombustibility, ultra-violet resistance, and material cost. However, CNTs mixed into cement composites for improving mechanical and electrical properties of the cement matrix, or to bring pressure-sensing (piezoresistive) properties to the composites (Chung 2001, Yu and Kwon 2009, Konsta-Gdoutos *et al.* 2010).

On the other hand, Geopolymers are amorphous aluminosilicate materials offer an environmentally friendly and technically competitive as well as alternative to ordinary Portland cement (OPC). The hardening mechanism involves the chemical reaction of Geopolymeric precursors, such as alumino-silicate oxides, with alkali polysilicates yielding polymeric Si-O-Al bonds. Production of Geopolymeric precursors carried out by calcinations of aluminosilicates natural clay materials. Their source can also be some industrial aluminosilicate waste materials (Laurenzi *et al.* 2013). As a means of converting waste materials to useful products, the value of geopolymer technology lies primarily in its ability to produce a high-performance binder from materials that are rich in silica and alumina oxides that are the bases of Geopolymerization process.

Geopolymer-based composites can be considered as an engineering application that can be reinforced with CNTs so that enhancing their mechanical properties, thermal resistance and so decreasing structure microporosity. Nowadays, Geopolymers considered as a replacement to ordinary Portland cement (OPC) and has received considerable attention for their cost efficiency, chemical stability, corrosion resistance, rapid strength gain rate, low shrinkage and freeze-thaw resistance (Kong *et al.* 2008, Bakharev 2004). However, due to their cross-linked structure, geopolymers tend to be more brittle than OPC and therefore, they are unsuitable for structural applications when safety-based structural design is considered. Geopolymers were found to be more brittle than OPC, and their fracture energy was about 40 % of that of OPC (Pan *et al.* 2011).

Several challenges must still be addressed in order to enhance the mechanical and electrical

Table 1 Chemical composition of starting materials (Mass, %)

Oxide content (%)	SiO <sub>2</sub>	Al <sub>2</sub> O <sub>3</sub>	Fe <sub>2</sub> O <sub>3</sub>	CaO	MgO	SO <sub>3</sub>	K <sub>2</sub> O	Na <sub>2</sub> O	TiO <sub>2</sub>	MnO	P <sub>2</sub> O <sub>5</sub>	Cl	SrO	BaO	L.O.I.	Total (%)
Air cooled Slag (ACS)	38.11	9.31	4.06	35.23	2.22	02.00	00.66	00.45	00.45	03.29	00.09	00.07	0.14	3.78	0.13	99.94
Water-Cooled Slag (GGBFS)	36.67	10.31	0.50	38.82	1.70	2.17	1.03	0.48	0.57	4.04	0.04	0.05	0.18	3.28	0.12	99.96
Fine Sand (Sand dunes)	89.91	2.00	1.45	1.56	1.91	0.87	0.37	0.06	0.03	0.04	0.03	0.12	-	-	1.65	99.98

properties of cement composites with CNTs; one of these is the effective dispersion of CNTs at the single tube level (Sanchez and Ince 2009, Gay and Sanchez 2010). CNTs known with high aspect ratios and strong van der Waals self-attraction between nanotubes, and tend to form CNT bundles (Sanchez and Ince 2009, Gay and Sanchez 2010). For enhancing CNTs dispersion in a cement matrix, many researchers have applied a sonication process with a water-soluble surfactant (Konsta-Gdoutos *et al.* 2010, Nam *et al.* 2010), however the surfactant applied in the sonication process can act as an air entraining agent, thereby generating entrapped pores in the cement matrix and ultimately degrading the mechanical properties of the cement composites (Nam *et al.* 2010).

Another major challenge is to improve the interfacial interaction between the CNTs and hydration products of cement (Kim *et al.* 2012). CNTs are expected to provide mechanical reinforcement between hydration products of cement with nano-scale dimensions (Yu and Kwon 2009), however hydration products (CSH), calcium hydroxide (CH), and ettringite have similar or larger size than CNTs, and only a few CNTs could be anchored by the hydration products in studies reported to date (Kim *et al.* 2012). Therefore, CNTs failed to reinforce the hydration products and, in mechanical terms, a large portion of CNTs in the cement matrix act as pores and cracks between the hydration products (Kim *et al.* 2012).

The purpose of the current study focused on investigating the thermal stability of slag Geopolymer mortars enhanced with MWCNT upon examining the mineralogical changes; firing shrinkage, differential thermo-gravimetric analysis and functionality of the resulted MWCNT reinforced geopolymeric nanocomposites mortars using FTIR as new multifunctional structural materials.

## 2. Experimental procedures

### 2.1 Materials

The materials, which used in this investigation, are ground granulated water cooled blast furnace slag (GGBFS), air cooled slag sourced from Iron and Steel Factory- Helwan, Egypt. The

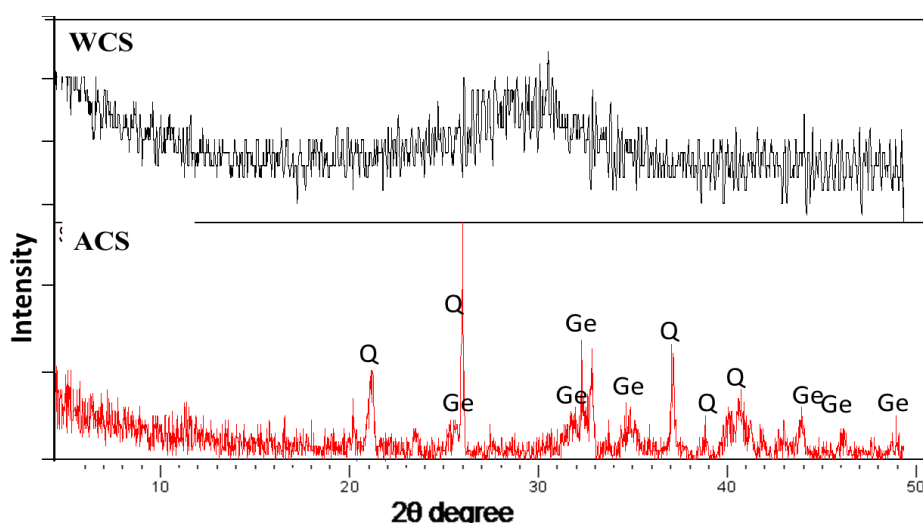


Fig. 1 Mineralogical composition of starting raw materials (Q: Quartz ( $\text{SiO}_2$ ), Ge: Gehlenite ( $\text{C}_2\text{ASH}_g$ ))

used sand dunes for mortar preparation sourced from fine sand (<1 mm) from Oases (Wahat)-Road, Egypt; however, their chemical compositions are tabulated in Table 1. The mineralogical composition represented in Fig. 1; where ground granulated blast furnace slag materials composed of amorphous constituents, while air cooled slag composed of crystalline minerals of quartz and gehlenite. Sodium hydroxide was used as alkali activators and produced by Fisher scientific company with 99 % purity.

Carbon Nano-tubes used for enhancing of geopolymeric mortar are of multiwall type consisting of many nested cylinders whose successive radii differ by roughly the interlayer spacing of graphite. Morphologies and microstructures of the as-synthesized carbon Nano materials were identified by transmission microscope (TEM), as shown in Fig. 2, which depicts a representative TEM image of as-synthesized carbon nanotubes deposited on 50% Co/ MgO by Acytelen gas decomposition at 700°C reaction temperature and ~ 4 hrs time-on-stream. These images show that, the morphologies have tubular structures, i.e., they are multi-walled carbon nanotubes (MWCNTs) and the boundaries between MWCNT tubes are clear. The diameters of the MWCNTs are mostly in the range of 14-24 nm. It is obvious in Fig. 2(a), (b) the dark object in the pictures is related to the Co- metal particles of the catalyst.

Raman spectroscopy used to estimate the degree of graphitization of the produced CNTs as represented in Fig. 2c; where there are two major bands observed, representing D- and G-bands. The D-band, at 1250-1350  $\text{cm}^{-1}$ , for the disorder induced due to the wall disorder or the presence of amorphous carbon deposited on the outer surface of nanotubes. The G-band (at 1550-1600  $\text{cm}^{-1}$ ) for the degree of graphitization of CNTs. The ratio of ID/IG of the D and G-band can be regarded as an index for the crystalline order of CNTs; the high ID/IG value (>1) indicates that there is high structural disorder in the carbon nanotubes obtained on the catalysts. However the lower ID/ IG value (<1) suggests the enhancement in graphitization of deposited carbon. The high intensity of the G-band (417  $\text{cm}^{-1}$ ) relative to D-band (270.7  $\text{cm}^{-1}$ ) (ID/IG ratio≈0.65) suggests that the CNTs synthesized under the optimum conditions were highly graphitized (Reich *et al.* 2004).

Thermo-gravimetric analysis (TGA) is also a very important tool for clarifying the yield, stability and quality of the as-grown MWCNTs, as indicated in Fig. 2d where the catalyst

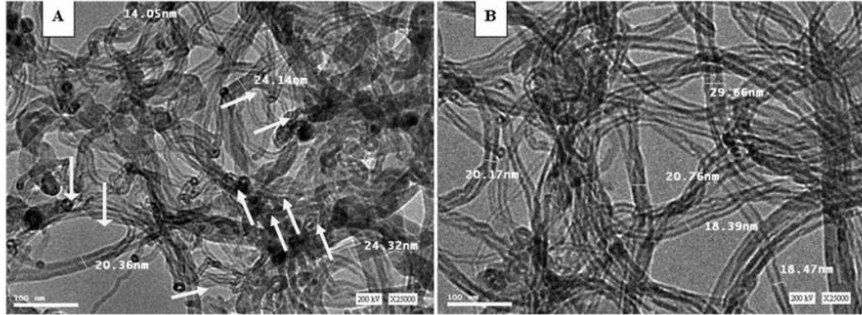


Fig. 2(a), (b) TEM pictures of catalysis after growth of CNT's using 50% Co/MgO catalyst, with high magnification

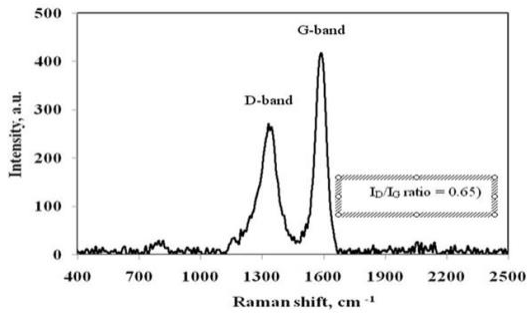


Fig. 2(c) Raman spectroscopy of CNTs over 50% Co/MgO catalyst

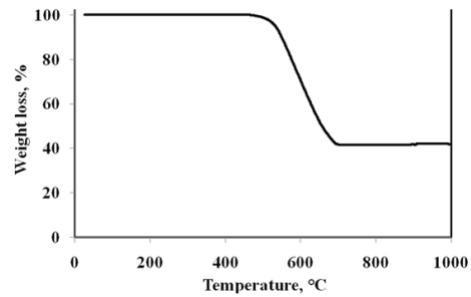


Fig. 2(d) Thermal gravimetric analysis after growth of CNTs using Co/MgO catalysis

Fig. 2 Characterization of synthesized multiwall carbon nano-tube

Table 2 Properties of CNTs synthesized by using CVD apparatus

Item	Property	Results
1	Outer diameter (nm)	20-30
2	Inner diameter (nm)	4
3	Purity wt. (%)	97
4	Length (mm)	1-5
5	Ash (%)	3
6	Amorphous (%)	0
7	Field (%)	800

presented a single oxidation inflection, indicating the low amorphous carbon and high purity MWCNTs are produced, also, TGA Data determine the onset, and offset (end) temperatures represent the temperature at the initial weight loss, (496°C) and the final weight loss, (692°C), respectively. The Large difference between the onset and end temperature (192) is to catalyst, which related to the formation of large diameters of CNTs, and proved by TEM photos (Fig. 2(a), (b)). Based on these results, the formation of ideal graphitized carbon Nano-materials and the highest carbon yield are gained on it. The properties of the produced MWCNT are summarized in Table 2.

## 2.2 Dispersion of MWCNTs

Because the strong Van der Waals forces cause Nano-particles agglomeration, a key issue in fabricating high-quality nanotube composite is to homogeneously disperse nano carbon materials in cementitious materials. Poor dispersion will lead to the formation of defects in the matrix and limit the nano-enhancement / modification effect (Ma *et al.* 2010). Many research works were done to improve the dispersion of nano carbon materials (NCM) in the cementitious composites. Commonly, there are two types of methods used to disperse NCMs. Mechanical separation of the NCMs by adopting ultrasonic which is one of the effective methods for CNT dispersion (Xie *et al.* 2005, Fu *et al.* 2001, Hamon *et al.* 2002). Currently, researchers have proposed some novel approaches for solving the NCMs dispersion. The first approach is to adopt commonly used water reducing admixtures (including plasticizers and superplasticizers) as surfactants. The research at the National Research Council Canada has shown that a small amount of CNTs can be dispersed by ultrasonication in 5% superplasticizer water containing mixture (Han *et al.* 2011). Shah *et al.* (2011) also achieved an effective dispersion of MWCNTs with different concentrations and lengths in cementitious materials by applying polycarboxylate-based superplasticizers.

In the present work MWCNTs were first mixed with Glenium Ace 30-polycarboxylate-based superplasticizer and 50% of the added water. This Polycarboxylate-based superplasticizer has been proven to be effective for CNTs dispersion (Collins *et al.* 2012). The solution was sonicated using a Fritish 450 Sonifier Analog Cell Distributor for 15 min (Weitzel *et al.* 2012). Solutions with concentration of 0.1, 0.2, 0.3, and 0.4-wt., % of the total weight of the matrix were used to evaluate of the threshold ratio of MWCNT.

## 2.3 Geopolymerization and curing

Alkaline activator composed of 6% NaOH, prepared 24 hrs prior to casting. The Geopolymer mortar reinforced with MWCNT concentrations: 0.0 (control), 0.1, 0.2, 0.3, and 0.4-wt., % of the total weight. Accordingly, mixing was performed by hand-mixing of used materials which grinded and passed a sieve of 90  $\mu\text{m}$  as represented in Table 3 according to the following sequence:

1. The previously prepared MWCNT particles sonicated for 15 min with 50% of the added water and the specified quantity of the superplasticizer for better dispersion of nanotubes materials under a temperature of 40°C.

2. The geopolymer materials were hand mixed with the alkaline solution dissolved in the remaining water content for 10 minute followed by a further 5 minute using rotary mixer, then mixed at medium speed (80 rpm) for another 30 s.

3. On the other hand, MWCNT and superplasticizer were added and stirred with mixture at high speed for additional 30 s.

4. The mixture was allowed to rest for 90 s and then mixed for 1 min at high speed.

Paste mixture was casted into 25×25×25 mm cubic-shaped moulds, vibrated for compaction, sealed with a lid to minimize any loss of evaporable water. All mixes were left cure undisturbed under ambient temperature for 24 hrs, demolded, and then subjected to curing at 40°C with 100% R.H. (El-Sayed *et al.* 2011). At the end of the curing regime, the specimens were subjected to compressive strength measurements, while the resulted crushed specimens exposed to stopping of the hydration process using stopping solution of methyl alcohol/acetone (1:1) followed by washing with acetone as recommended by different investigators (El-Sayed *et al.* 2011, Saikia *et al.* 2004) to prevent further hydration and for further analysis followed by drying of the crushed specimens

Table 3 Composition of the geopolymer mixes (Mass, %)

Mix no.	Water cooled slag, %	Air cooled slag, %	Sand dunes, %	MWCNT addition from the added binder, %	W/B ratio, %	Super-plasticizer of the total wt., %
R	16.7	16.7	66.6	0.0	0.34	1.4
1	16.7	16.7	66.6	0.1	0.34	1.6
2	16.7	16.7	66.6	0.2	0.34	1.8
3	16.7	16.7	66.6	0.3	0.39	2.0
4	16.7	16.7	66.6	0.4	0.39	2.2

for 24 hrs at 80°C, then preserved in a well tight container until the time of testing.

Firing resistant measurement was carried out by curing at 40°C and 100% R.H. for 28 days, and then the samples were removed from their curing regime, dried at 80°C for 24 hrs, then calcined at different temperatures (200-1000°C) for 2 hrs with a heating rate of 5°C/min (Wenying *et al.* 2008).

## 2.4 Methods of investigation

Axios (PW4400) WD-XRF Sequential Spectrometer (Panalytical, Netherland) used for chemical analysis of the starting raw materials. Compressive strength tests were carried out using five tones German Bruf pressing machine with a loading rate of 100 kg/min determined according to ASTM C109M(2012). XRD analysis was recorded on a Philips PW 1050/70 Diffractometer using a Cu-K $\alpha$  source with a post sample K $\alpha$  filter. XRD patterns were collected from 0° to 50° 2 $\theta$  (step size 0.02 °2 $\theta$  and speed 0.4°/min). Silica was used as an internal standard. Data were identified according to the XRD software (pdf-2: database on CD-Release 2005). Removal of free water was accomplished by using methyl alcohol/acetone method as recommended by different investigators (El-Sayed *et al.* 2011, Saikia *et al.* 2004).

Firing shrinkage test was carried out on dried samples at 110°C for 24 hrs to ensure total water loss. The test specimens were then measured (in terms of dimension) and their values were noted as dry lengths. The test specimens were also fired in an electric furnace to the desired firing temperature and then allowed to cool, and then specimens were weighted and measured, while the fired lengths were recorded. The firing shrinkage was calculated for each test specimen using the following formula (Norsker 1987, Ugheoke *et al.* 2006)

$$\% \text{ Average Firing Shrinkage} = (DL-FL)/FL * 100 \quad (2)$$

where: DL stands for dry length and FL is fired length.

Bonding characteristics of the alkali activated specimens were analyzed using a Jasco-6100 Fourier transformed infrared spectrometer FTIR. Test sample was ground and uniformly mixed with KBr at a weight ratio KBr: specimen=200:1. The mixture, 0.2 g was pressed to a disk of 13 mm in diameter for analysis at 8 t/cm<sup>2</sup>. The wave number was ranging from 400 to 4000 cm<sup>-1</sup> (Paniyas *et al.* 2007, Alexandre Silva *et al.* 2013).

Thermogravimetry conducted using DT-50 Thermal Analyzer (Schimadzu Co-Kyoto, Japan). Samples were crushed, transferred immediately to an alumina crucible, held under isothermal conditions for 60 min at 40°C to equilibrate in a nitrogen environment (N<sub>2</sub> flowing at 200 ml/min), and then heated to 1000°C at 10°C/min in the same gas environment.

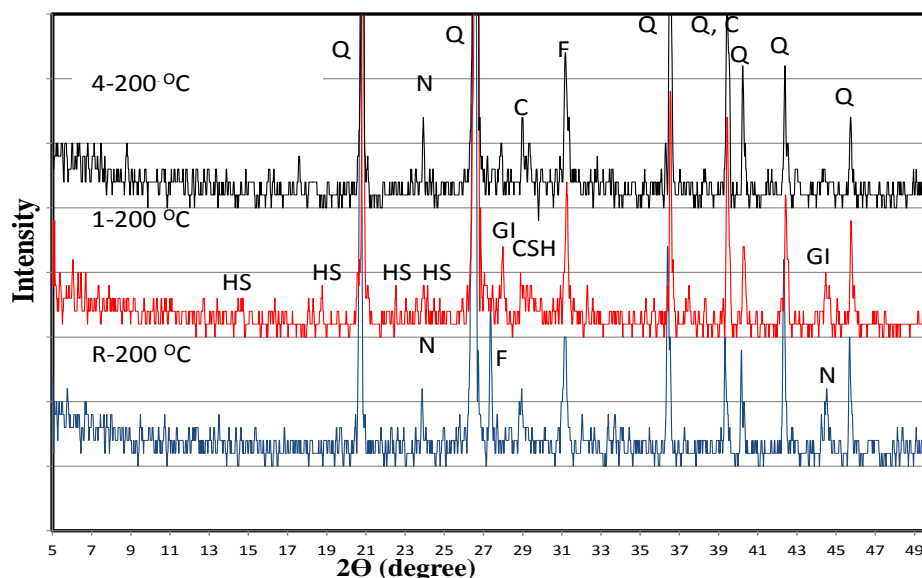


Fig. 3 XRD pattern of geopolymer mortar mixes having various doses of NWCNT fired at 200 °C (Q: Quartz, F: Feldspar, N (Nepheline):  $\text{NaAlSi}_3\text{O}_8$ , C: Calcite, CSH: Calcium silicate hydrate, Gi: Gismondine, HS: Hydroxysodalite)

### 3. Results and discussion

The mineralogical patterns of geopolymer mortar mixes having 0, 0.1 and 0.4% MWCNT, fired at 200 °C using XRD are shown in Fig. 3. All samples provide a broad band in the region of 6-10° 2θ for aluminosilicate gel and broad bands in the region of 17-35° 2θ which is for the glassy phase of the geopolymer component, both increase with MWCNT up to 0.1% giving an indication about an increased enhancement in the produced geopolymer structure, however, further increase in MWCNT results in the agglomeration and bundling of nanomaterials, so hinder the propagation of the three-dimensional geopolymer network. It can be noticed also an increase in the broadness and intensity of the CSH band up to 0.1%, at 29.4° which is in coherent with other studies (Ben Haha *et al.* 2011), where the incorporated MWCNTs increase the hydration speed after addition to the same system.

Also, MWCNTs provide different nucleation sites for the crystal growth, as known from literature where the hydration products grow on the surface of carbon nanotubes (Jiang *et al.* 2005, Chen and Poon 2009). CSH-phases bind to the MWCNTs at the Carboxyl-sites by interaction of the  $\text{Ca}^{2+}$ -ions of the pore solution, therefore the carboxyl group-density on the surface of the MWCNTs can influence the chain lengths of the grown CSH-phases.

The increase in CSH-phases is so attributed to the effect of the NaOH alkaline solution during processing. However, CSH structure formed in the presence of highly concentrated NaOH was less dense than the normal CSH resulting from the hydration of Portland cement as reported by Bakharev *et al.* (1999).

The control mortar without MWCNT shows the formation of semi-crystalline geopolymer nepheline in addition to a lower extent of CSH as well as excess carbonate content, which is attributed to the lower reactivity of the formed geopolymer structure as well as increased porosity as

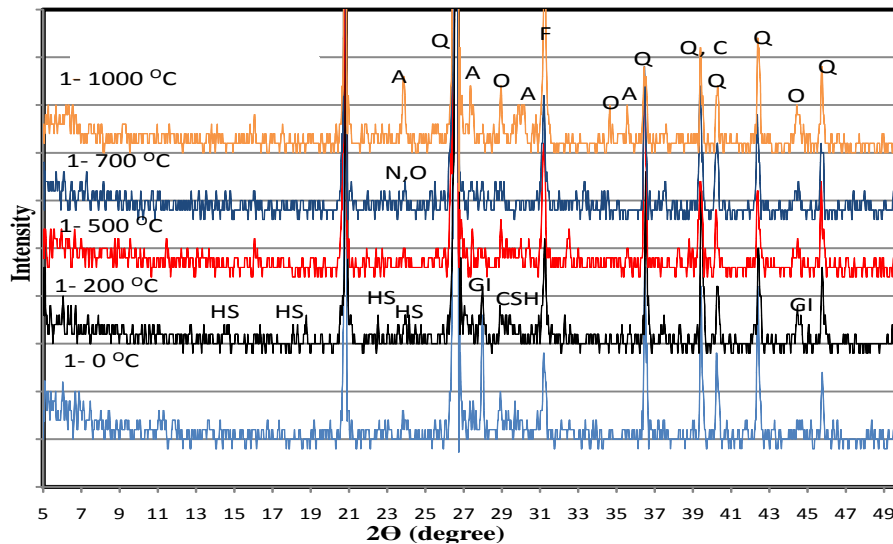


Fig. 4 XRD pattern of geopolymer mortar mixes having 0.1% addition of MWCNT and fired at different firing temperatures (Q: Quartz, F: Feldspar, N (Nepheline):  $\text{NaAlSiO}_4$ , O:  $\text{NaAlSi}_2\text{O}_6$ , A (Albite):  $\text{NaAlSi}_3\text{O}_8$ , C: Calcite, Gi: Gismondine, HS: Hydroxysodalite)

compared with 0.1% MWCNT which form amorphous aluminosilicate gel with the formation of semi-crystalline hydroxysodalite and Na-P1 (Gismondine) zeolite upon firing at 200°C, and possess further binding in the matrix network as the inner binding product formed around partially reacted slag particles after firing to 200°C (Ben Haha *et al.* 2011). However, increasing the MWCNT to 0.4% results in the formation of Na-feldspars  $\text{AlNa}(\text{SiO}_4)$  nepheline, giving an indication about the lower reactivity and stability of the formed geopolymer structure which transformed into the crystalline one.

Fig. 4 presents the mineralogical identification upon exposure to firing at 0, 200, 500, 700 and 1000°C for geopolymer mortar doped with 0.1% MWCNT, where traces of amorphous aluminosilicate gel and semi-crystalline hydroxysodalite as well as Na-P1 (Gismondine) zeolite formed at 200°C, reflecting the activation of geopolymer structure and enhancing the bonding characteristics by MWCNT materials, in addition to, thermal activation of the resulted CSH. On firing at 500°C, peaks for hydroxysodalite as well as Na-P1 (Gismondine) disappeared, while crystalline nepheline  $\text{AlNaSiO}_4$  formed. Increasing temperature to 1000°C, results in the formation of slightly traces of  $\text{NaAlSi}_2\text{O}_6$ , while strong peaks for albite  $\text{NaAlSi}_3\text{O}_8$  in addition to Na-feldspars  $\text{AlNa}(\text{SiO}_4)$  and  $\text{NaAlSi}_2\text{O}_6$ , formed. The formed crystalline feldspars reflecting the reactivity decline of the geopolymer constituents as well as the lower stability of the formed mortar beyond 200°C.

FTIR spectra of alkali-activated geopolymer mortars have a bands description as follow: stretching vibration of O-H bond at about 3430, 1600  $\text{cm}^{-1}$ , stretching vibration of  $\text{CO}_3^{2-}$  located at about 1410  $\text{cm}^{-1}$ , asymmetric stretching vibration (Si-O-Si) related to non-solubilized particles at about 1100  $\text{cm}^{-1}$ , asymmetric stretching vibration (T-O-Si) at about 975  $\text{cm}^{-1}$  where T=Si or Al, symmetric stretching vibration of  $\text{CO}_3^{2-}$  at about 870  $\text{cm}^{-1}$ , symmetric stretching vibration of (Si-O-Si) attributed to  $\alpha$ -quartz at about 797  $\text{cm}^{-1}$ , symmetric vibration at about 778  $\text{cm}^{-1}$  for (Al-O-Si), symmetric stretching vibration (Si-O-Si) in the region 676-700  $\text{cm}^{-1}$  and bending vibration (Si-O-

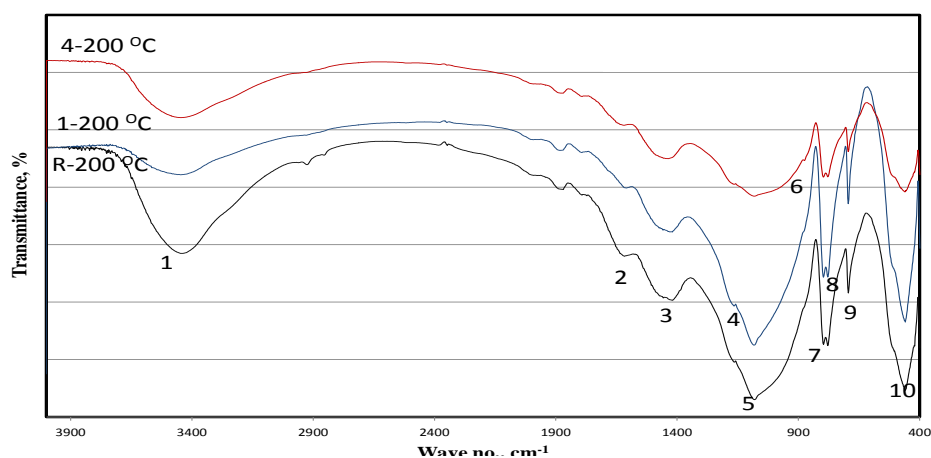


Fig. 5 FTIR spectra of geopolymers mortar specimens having various MWCNT content fired at 200°C (1: Stretching vibration of O-H bond, 2: Bending vibrations of (HOH), 3: Stretching vibration of CO<sub>2</sub>, 4: Asymmetric stretching vibration (Si-O-Si), 5: Asymmetric stretching vibration (T-O-Si), 6: Symmetric stretching vibration of CO<sub>2</sub>, 7: Symmetric stretching vibration (Si-O-Si) attributed to  $\alpha$ -quartz, 8: Symmetric stretching vibration of (Al-O-Si), 9: Symmetric stretching vibration (Si-O-Si), 10: Bending vibration (Si-O-Si and O-Si-O)

Si and O-Si-O) in the region of 430-445 cm<sup>-1</sup> (Alexandre Silva *et al.* 2013).

FTIR spectra of alkali-activated geopolymer mortar mixes containing 0, 0.1 and 0.4% MWCNT fired at 200°C, Fig. 5, indicate increase in broadness of the asymmetric band at 975 cm<sup>-1</sup> up to 0.1 % -confirming hydroxysodalite formation as represented in XRD pattern (Fig. 3)-which assigned to a combination of the Si-O-T vibration of N-A-S-H, asymmetric stretching of Na-X 980 cm<sup>-1</sup>, and of hydroxysodalite at 979 cm<sup>-1</sup> (Chukanov 2014); this increase accompanied by a decrease in the asymmetric band at about 1100 cm<sup>-1</sup> for nonsolubilized slag particles giving an indication about increased dissolution of the unreacted materials with thermal firing to 200 degree which positively reflected on increased amorphous constituents (Alexandre Silva *et al.* 2013). An increased broadness and intensity of CSH band at about 3400 cm<sup>-1</sup> is in agreement with XRD data interpretation (Fig. 3). On the other hand, firing of geopolymer mix incorporated with 0.4 % MWCNT subjected to a sharp decrease in the asymmetric band as well as shifting to a higher wave number as the amorphous constituents transferred into crystalline zeolitic one.

Carbonate bands in the regions of 1430 cm<sup>-1</sup> ( $\nu$  C-O) as well as 867 cm<sup>-1</sup> ( $\delta$  C-O) appeared to be in the same intensity, as carbonate constituents in slag materials share in the formation of carbonate band as discussed above, showing that the carbonates identified in this raw material do not react significantly under alkaline medium (Susan *et al.* 2012).

FTIR spectra of alkali-activated geopolymer mortar mixes having 0.1% MWCNT, fired at different firing temperatures from 0, 200 up to 1000°C Fig. 6, illustrate an increase in asymmetric band with firing to 200°C as a result of activation of geopolymer structure and increased content of N-A-S-H as well as C-A-S-H. However, further increase in firing temperature leads to dehydroxylation of geopolymer's three dimensional structure as well as C-S-H and so decrease in intensity of asymmetric band in addition to shift into higher wave number values confirming transformation of the amorphous constituents into crystalline one; also this shift increases with firing up to 1000 degree as the transformation of the amorphous into crystalline zeolite

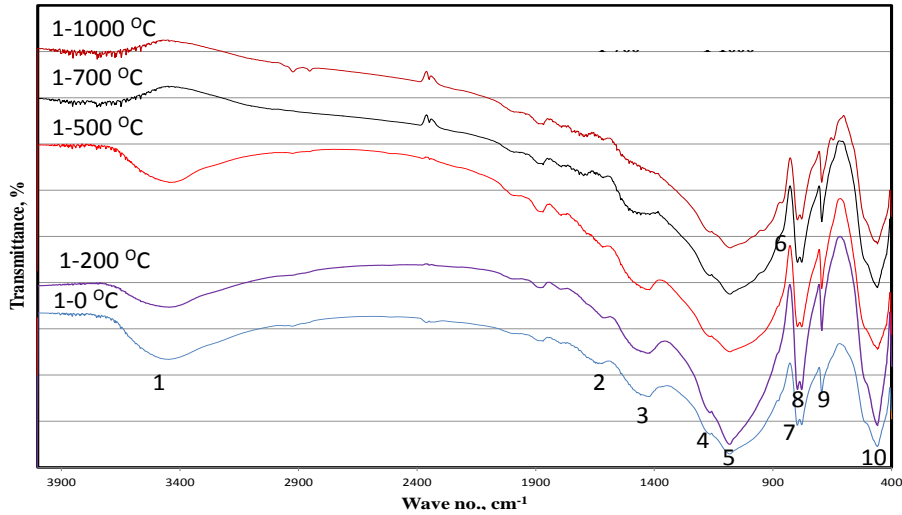


Fig. 6 FTIR spectra of geopolymer mortar specimens having 0.1% addition of MWCNT content, fired at various firing temperatures. (1: Stretching vibration of O-H bond, 2: Bending vibrations of (HOH), 3: Stretching vibration of CO<sub>2</sub>, 4: Asymmetric stretching vibration (Si-O-Si), 5: Asymmetric stretching vibration (T-O-Si), 6: Symmetric stretching vibration of CO<sub>2</sub>, 7: Symmetric stretching vibration (Si-O-Si) attributed to  $\alpha$ -quartz, 8: Symmetric stretching vibration of (Al-O-Si), 9: Symmetric stretching vibration (Si-O-Si), 10: Bending vibration (Si-O-Si and O-Si-O)

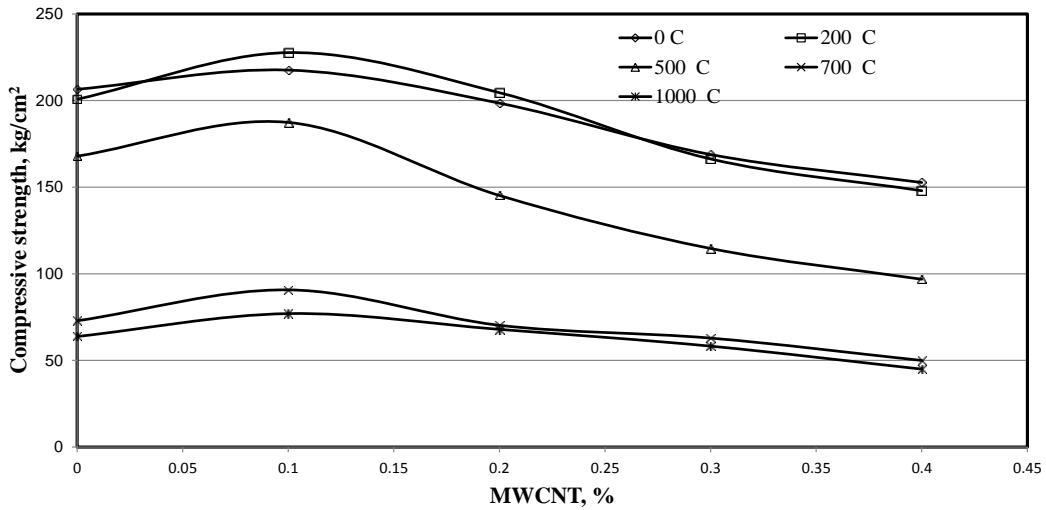


Fig. 7 Compressive strength of alkali activated geopolymer mortar specimens doped with various doses of MWCNT fired at various firing temperatures

constituents increase. The CO<sub>3</sub><sup>2-</sup> vibration band decreases with firing temperature as a result of decalcification until vanishing at 1000°C.

Fig. 7 illustrate compressive strength of geopolymer mixes enhanced with MWCNTs, fired at different temperatures from 0 to 1000°C, where a decrease in the compressive strength with temperature up to 1000°C except for mixes having 0.1 and 0.2% MWCNT and fired at 200 degree.

Results show a decrease in mechanical strength as clarified from strength change factors (as compared with unfired 28 days geopolymer mortar specimens) at 200°C are 2.78%, -4.63%, -3.05% and 3.11%, while reaching to 18.69, 13.88, 26.84, 36.57% at 500°C upon using 0, 0.1, 0.2 and 0.4% MWCNT, respectively. Further increase in firing temperature leads to an increase in strength loss which negatively affects the stability of the thermally treated geopolymer mortar, also the lower firing shrinkage accompanied by using 0.1% MWCNT was observed specially at 200 degree; where, the increase in positive change factor means a dramatic decrease in strength, while negative values signify a strength increase, as coincide with XRD and FTIR (Figs. 3-6), and confirm presence of amorphous geopolymer chains up on firing and little evidence of the formation of crystalline zeolite structure.

However, strength decrease explained also by increased dehydroxylation of the geopolymer networks leading to the decomposition of the geopolymer structure and so more porous structure formed as well as rapid increase of the average pore size resulting in the formation of microcracks as the vitreous structures replaced by the crystalline Na-feldspars; and in turn increase in porosity and strength deterioration (Bakharev 2006).

Geopolymer mix of 0.1 and 0.2% MWCNT exhibits a remarked withstand against firing to 200°C compared with other CNT- geopolymer mixes as the formation of amorphous aluminosilicate gel and semi-crystalline hydroxysodalite as well as Na-P1 (Gismondine) zeolite is predominant, which positively reflected on compressive strength (Alexandre Silva *et al.* 2013), this is in addition to good dispersion of individual MWCNTs throughout the geopolymer matrix with a uniform density.

The good dispersion of MWCNTs also attributed to the effect of the NaOH alkaline solution during processing as discussed (Heister *et al.* 2010) and hydrophilic groups (-COOH) in carboxylate based super-plasticizer forming covalence-modified CNTs to improve interfacial interactions in composites, in which the -COOH groups form strong coordinate bonds with the Ca<sup>2+</sup> ions in matrix, thus enhancing the formation of three dimensional geopolymer in addition to CSH (Li *et al.* 2005, Susan *et al.* 2012). Furthermore, the addition of CNTs fines the pore size with microporosity decrease (or nanoporosity) of composites by filling the gaps (or pores) between the hydration products such as CSH gel geopolymer composite. Therefore, the composites become much more compacted (Han *et al.* 2011, Chen *et al.* 2011) and with more stability to firing up to 200°C.

The increased strength loss beyond 0.2% MWCNT, reflects the lower thermal stability of the resulted products where the carboxylate based superplasticizer was ineffective in dispersing MWCNTs at 0.3- wt., % and more, where most of MWCNT agglomerated in the alumino-silicate gel forming more microcracks as well as hinder the propagation of the three dimensional network.

The firing shrinkage pattern of the geopolymer mortar specimens with various MWCNT ratios and fired at different temperature up to 1000°C is shown in Fig. 8, where a decrease in shrinkage with MWCNT up to 0.1% at all firing temperatures up to 500°C is observed, however the shrinkage values increase with temperature up to 500°C. Further increase on the firing temperature up to 1000°C results in an increase in volume due to expansion resulted from increased transformation of amorphous into crystalline zeolite, as the lower melting point reflects the high shrinkage (Norsker 1987, Ugheoke *et al.* 2006).

The firing shrinkage values of geopolymer mortar with MWCNT coincided with previous findings stated that beyond 200°C, as minor or no shrinkage or expansions were recorded until 500°C. Between 500°C and 1000°C, an increase in shrinkage was observed. Increase in shrinkage occurred also due to mass loss in geopolymer when subjected to elevated temperature. Since

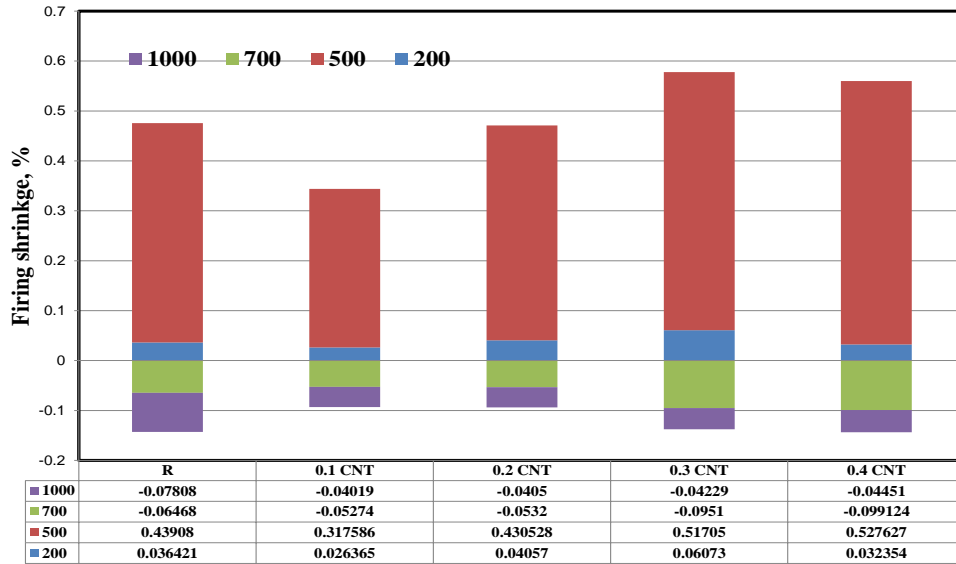


Fig. 8 Firing shrinkage of geopolymer mortar mix with various ratios of MWCNT as a function of firing temperature

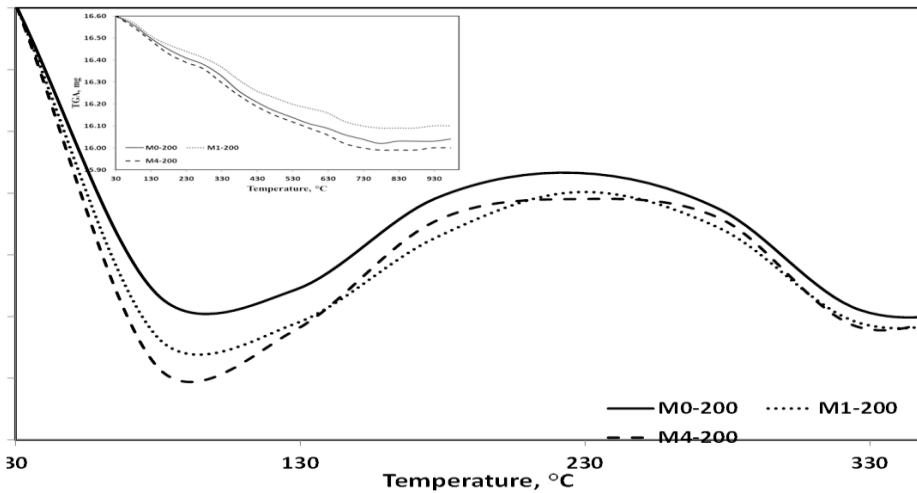


Fig. 9 Differential thermogravimetric analysis of alkali activated geopolymer mortars doped with various doses of MWCNT and fired at 200°C

mortars required for OPC patch repair require very low shrinkage up to 200 degree, this means that new geopolymeric mortar mixtures with lower expansion values up to 200 degree incorporating 0.1 and 0.2% MWCNT can be used as a repair mortar.

Thermogram of the geopolymer mortar incorporate various ratios of MWCNT (Fig. 9) after thermal firing to 200°C showed a weight loss at temperatures lower than 300°C, associated with the physically bound and zeolitic water in the reaction products (Duxson *et al.* 2007). The main peak identified presents a minimum at ~103°C, related to freely evaporable water present in large

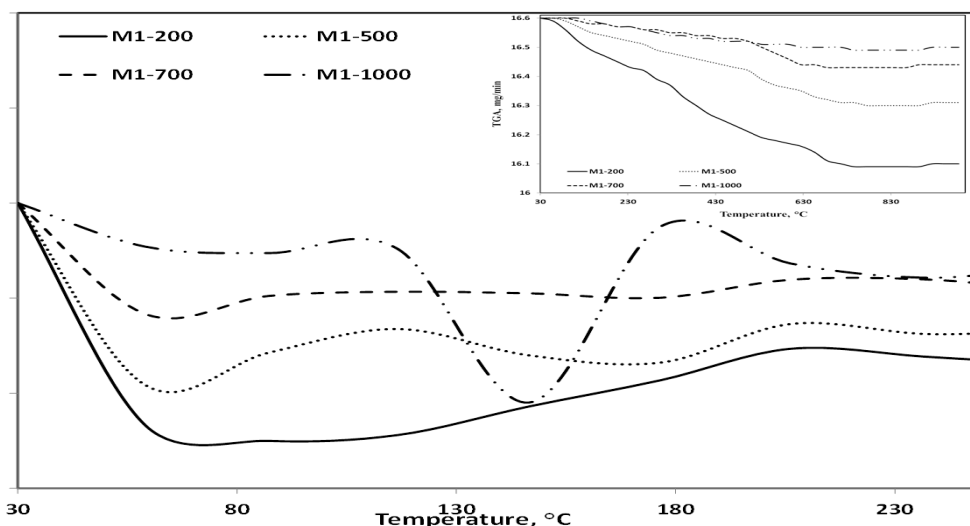


Fig. 10 Differential thermogravimetric analysis of alkali activated geopolymer mortars doped with various doses of MWCNT and fired at various firing temperatures

geopolymer gel pores, where an increased intensity of this peak in samples containing 0.1% MWCNT than higher doses reflects increasing of aluminosilicate gel formation, which in agreement with the high compressive strength values identified in mortar prepared with this binder.

Comparing samples with different MWCNTs at 200°C, where geopolymers without nanotube gives a total weight loss of ~3.37%, 0.1% geopolymers presented ~3.11% loss, and 0.4% geopolymer mix gives a loss of 3.77%.

The lower weight loss by using 0.1% MWCNT confirms the lower water content. The higher loss observed also at higher nanotube content, reflecting the increased agglomeration and porosity up on using this high ratio, as identified by FTIR and XRD.

On comparing thermograms of geopolymer mortar fired at different temperature on and contains 0.1% MWCNT (Fig. 10), an increase in the intensity of the peak at ~146°C associated with the dehydration of the zeolite-type product (albite) formed along with the geopolymer gel <~103 degree (Bernal *et al.* 2011). The decrease in the peak intensity of the geopolymer gel was noticed from a broad one upon firing at 200°C to a narrow peak at 1000°C, accompanied by an increase in the zeolite peak intensity.

Crystalline zeolites weight loss has been reported at temperatures of ~175°C for nepheline which decrease with temperature up to 1000°C, while pronounced increase in the albite peak of zeolite at about 146°C observed. The total weight losses were ~3.11, 1.85, 1.1 and 0.61 up on firing at 200, 500, 700, and 1000°C, respectively, where the decrease in the total loss with temperature reflects the increase in the degree of dehydroxylation up to 1000°C which is in consistent with the difference in water content between crystalline forms of zeolite.

The investigation showed that the prepared geopolymer materials compared favorably with organic polymers, they are nonflammable, do not release toxic fumes and have very low weight loss <4% as compared to 50-80% for fire-resistant polymer nanocomposites when heated up to 1000°C.

#### 4. Conclusions

1. Adding MWCNT to alkali activated geopolymer mortar specimens' increases and offers an extra nucleation sites for geopolymer formation and accumulation up to 0.1%.

2. XRD and FTIR of fired mortar nanocomposites with 0.1 up to 0.4 wt., % MWCNT at 200°C showed an increase in the amorphous geopolymer content up to 0.1% as well as increased broadness and intensity of CSH band, while zeolitic structure increase with temperature increase.

3. Strength change factors are (as compared with unfired 28 days) at 200°C are 2.78%, -4.63%, -3.05% and 3.11%, while reaching to 18.69, 13.88, 26.84, 36.57% at 500°C upon using 0, 0.1, 0.2 and 0.4% MWCNT, respectively. The latter ratios increase with the increase in firing temperatures up to 1000°C.

4. DTG showed an increased broadness of freely evaporable water in the geopolymer gel up to 200 degree using 0.1% MWCNT, while the increase in firing temperature results in the increase in the zeolite peak up to 1000°C.

5. The investigation showed that prepared geopolymer materials compared favorably with organic polymers, they are nonflammable, do not release toxic fumes and have very low weight loss < 4% as compared to 50-80% for fire-resistant polymer nanocomposites when heated up to 1000°C.

6. It is known that mortars required for OPC patch repair require very low shrinkage up to 200 degree, so the new geopolymeric mortar mixtures with lower expansion values up to 200 degree incorporating 0.1 and 0.2% MWCNT can be used as a repair mortar.

#### References

- ASTM C109M-12 (2012), Standard Test Method for Compressive Strength of Hydraulic Cement Mortars.
- Bakharev, T. (2004), "Resistance of geopolymer materials to acid attack", *Cement Concrete Res.*, **35**(4), 658-70.
- Bakharev, T. (2006), "Thermal behavior of geopolymer prepared using class F fly ash and elected temperature curing", *Cement Concrete Res.*, **36**,1134-1147.
- Bakharev, T., Sanjayan, J.G. and Cheng, Y.B. (1999), "Effect of elevated temperature curing on properties of alkali-activated slag concrete", *Cement Concrete Res.*, **29**, 1619-1625.
- Ben Haha, M., Le Saout, G., Winnefeld, F. and Lothenbach, B. (2011), "Influence of activator type on hydration kinetics, hydrate assemblage and microstructural development of alkali activated blast-furnace slags", *Cement Concrete Res.*, **41**(3), 301-10.
- Ben Haha, M., Lothenbach, B., Le Saout, G. and Winnefeld, F. (2011), "Influence of slag chemistry on the hydration of alkali-activated blast-furnace slag-Part I: effect of MgO", *Cement Concrete Res.*, **41**(9), 955-63.
- Bernal, S.A., Rodriguez, E.D., de Gutierrez, R.M., Gordillo, M. and Provis, J.L. (2011), "Mechanical and thermal characterization of geopolymers based on silicate activated metakaolin/slag blends", *J. Mater. Sci.*, **46**(16), 5477-86.
- Bernal, S.A., Rodríguez, E.D., de Gutiérrez, R.M., Provis, J.L. and Delvasto, S. (2012), "Activation of metakaolin/slag blends using alkaline solutions based on chemically modified silica fume and rice husk ash", *Waste Biomass Valor*, **3**, 99-108.
- Bi, S., Su, X., Hou, G., Liu, C., Song, W.L. and Cao, M.S. (2013), "Electrical conductivity and microwave absorption of shortened multi-walled carbon nanotube/alumina/ceramic composites", *Ceram Int.*, **39**(5), 5979-83.
- Chen, S.J., Collins, F.G., Macleod, A.J.N., Pan, Z., Duan, W.H. and Wang, C.M. (2011), "Carbon nanotube-

- cement: a retrospect”, *ISE J. Part A: Civil Struct. Eng.*, **4**(4), 254-65.
- Chen, J. and Poon, C. (2009), “Photocatalytic construction and building materials: From fundamentals to applications”, *Build. Envir.*, **44**(9), 1899-1906.
- Chukanov, N. (2014), *Infrared spectra of mineral species*, Springer.
- Chung, D.D.L. (2001), “Comparison of submicron-diameter carbon filaments and conventional carbon fibers as fillers in composite materials”, *Carbon.*, **39**(8), 1119-25.
- Collins, F., Lambert, F. and Duan, W.H. (2012), “The influence of admixtures on the dispersion, workability, and strength of carbon nanotube-OPC paste mixtures”, *Cement Concrete Compos.*, **34**(9), 1067-74.
- de Vargas, A.S., Dal Molin, D.C., Masuero, A.B., Vilela, A.C., Castro-Gomes, J. and de Gutierrez, R.M. (2014), “Strength development of alkali-activated fly ash produced with combined NaOH and CA(OH)<sub>2</sub> activators”, *Cement Concrete Compos.*, **53**, 341-349.
- Duxson, P., Lukey, G.C. and van Deventer, J.S.J. (2007), “The thermal evolution of metakaolin geopolymers: Part 2-phase stability and structural development”, *J. Non-Cryst. Solid.*, **353**, 2186-200.
- El-Sayed, H.A., Abo El-Enein, S.A., Khater, H.M. and Hasanein, S.A. (2011), “Resistance of alkali activated water cooled slag geopolymer to sulfate attack”, *Ceramics-Silikaty*, **55**, 153-160.
- Fakhru’l-Razi, A., Atieh, M.A., Girun, N., Chuah, T.G., El-Sadig, M. and Biak, D.R.A. (2006), “Effect of multi-wall carbon nanotubes on the mechanical properties of natural rubber”, *Compos. Struct.*, **75**(1-4), 496-500.
- Fu, K., Huang, W. and Lin, Y. (2001), “Defunctionalization of functionalized carbon nanotubes”, *Nano Lett.*, **1**(8), 439-441.
- Gao, D., Sturm, M. and Mo, Y. (2009), “Electrical resistance of carbon-nanofiber concrete”, *Smart Mater. Struct.*, **18**, 095039.
- Gay, C. and Sanchez, F. (2010), “Performance of carbon nanofiber-cement composites with a high-range water reducer”, *Transp. Res. Rec., J. Tran. Res. Board.*, **2142**, 109-13.
- Hamon, M.A., Hui, H. and Bhowmik, P. (2002), “Ester-functionalized soluble single-walled carbon nanotubes”, *Appl. Phys. A.*, **74**(3), 333-338.
- Han, B., Yu, X. and Ou, J. (2011), *Multifunctional and smart carbon nanotube reinforced cement-based materials, Nanotechnology in Civil Infrastructure*, Springer.
- Han, B., Yang, Z. and Shi, X. (2013), “Transport properties of carbon-nanotube/cement composites”, *J. Mater. Eng. Perform.*, **22**(1), 184-189.
- Heister, E., Lamprecht, C., Neves, V., Tilmaciu, C., Datas, L. and Emmanuel Flahaut, E. (2010), “Higher dispersion efficacy of functionalized carbon nanotubes in chemical and biological environments”, *ACS Nano*, **4**(5), 2615-26.
- Huang, S. (2012), “Multifunctional graphite nanoplatelets (GNP) reinforced cementitious composites”, Dissertation for the Degree of Master of Engineering, National University of Singapore, Singapore.
- Jiang, X., Kowald, T., Staedler, T. and Trettin, R. (2005), “Carbon nanotubes as a new reinforcement material for modern cement-based binders”, *RILEM Proceedings, 2nd International Symposium on Nanotechnology in Construction*, 209-213.
- Khalili, S.M.R. and Haghbin, A. (2013), “Investigation on design parameters of single-walled carbon nanotube reinforced nanocomposites under impact loads”, *Compos. Struct.*, **98**, 253-60.
- Kim, H.K., Nam, I.W. and Lee, H.K. (2012), “Microstructure and mechanical/EMI shielding characteristics of CNT/cement composites with various silica fume contents”, *UKC 2012 on Science, Technology, and Entrepreneurship*, California, USA, August.
- Kong, D.L.Y. and Sanjayan, J.G. (2008), “Damage behaviour of geopolymer composites exposed to elevated temperatures”, *Cement Concrete Compos.*, **30**(10), 986-91.
- Konsta-Gdoutos, M.S., Metaxa, Z.S. and Shah, S.P. (2010), “Highly dispersed carbon nanotubes reinforced cement based materials”, *Cement Concrete Res.*, **40**(7), 1052-9.
- Konsta-Gdoutos, M.S., Metaxa, Z.S. and Shah, S.P. (2010), “Multi-scale mechanical and fracture characteristics and early-age strain capacity of high performance carbon nanotube/cement nanocomposites”, *Cement Concrete Compos.*, **32**(2), 110-5.
- Laurenzi, S., Pastore, R., Giannini, G. and Marchetti, M. (2013), “Experimental study of impact resistance in

- multi-walled carbon nanotube reinforced epoxy”, *Compos. Struct.*, **99**, 62-8.
- Li, G., Wang, P. and Zhao, X. (2005), “Mechanical behavior and microstructure of cement composites incorporating surface-treated multi-walled carbon nanotubes”, *Carbon*, **43**(6), 1239-1245.
- Ma, P.C., Siddiqui, N.A. and Marom, G. (2010), “Dispersion and functionalization of carbon nanotubes for polymer-based nanocomposites: a review”, *Compos. Part A: Appl. Sci. Manuf.*, **41**(10), 1345-1367.
- Makar, J., Margeson, J. and Luh, J. (2005), “Carbon nanotube/cement composites-early results and potential applications”, *3rd International Conference on Construction Materials: Performance, Innovations and Structural Implications*, Vancouver, August.
- Mukhopadhyay, A.K. (2011), *Next-generation nano-based concrete construction products: a review, Nanotechnology in Civil Infrastructure*, Springer Berlin Heidelberg.
- Nam, I.W., Kim, H.K. and Lee, H.K. (2010), “Investigation of high-strength and electromagnetic wave shielding properties of a mortar incorporating carbon nanotube (CNT)”, *IV European conference on computational mechanics (ECCM IV)*, Paris, France, May.
- Norsker, H. (1987), *The Self-reliant potter: refractories and kilns*, Vieweg&Sohn, Friedr, Braunschweig/Wiesbaden.
- Pacheco-Torgal, F., Domingos, M., Ding, Y. and Jalali, S. (2011), “Composition, strength and workability of alkali-activated metakaolin based mortars”, *Construct. Build. Mater.*, **25**, 3732-3745.
- Pan, Z., Sanjayan, J.G. and Rangan, V. (2011), “Fracture properties of geopolymer paste and concrete”, *Mag. Concrete Res.*, **63**(10), 763-71.
- Panias, D., Giannopoulou, I.P. and Perraki, T. (2007), “Effect of synthesis parameters on the mechanical properties of fly ash-based geopolymers”, *Coll. Surf. A: Physicochem. Eng. Aspect.*, **301**, 246-254.
- Parveen, S., Rana, S. and Fanguero, R. (2013), “A review on nanomaterial dispersion, microstructure and mechanical properties of carbon nanotube and nanofiber reinforced cementitious composites”, *J. Nanomater.*, Article No. 80, 71017580.
- Raki, L., Beaudoin, J. and Alizadeh, R. (2010), “Cement and concrete nanoscience and nanotechnology”, *Mater.*, **3**(2), 918-942.
- Reich, S., Thomsen, C. and Maultzsch, J. (2004), *Carbon Nanotubes: Basic Concepts and Physical Properties*, Wiley-VCH, Germany.
- Walters, D.A. (1999), “Elastic strain of freely suspended single-wall carbon nanotube ropes”, *Appl. Phys. Lett.*, **74**, 3803-5.
- Saikia, N., Usami, A., Kato, S. and Kojima, T. (2004), “Hydration behavior of ecocement in presence of metakaolin”, *Res. Prog. J.*, **51**, 35-41.
- Sanchez, F. and Ince, C. (2009), “Microstructure and macroscopic properties of hybrid carbon nanofiber/silica fume cement composites”, *Compos. Sci. Technol.*, **69**(7-8), 1310-8.
- Sanchez, F. and Sobolev, K. (2010), “Nanotechnology in concrete-a review”, *Construct. Build. Mater.*, **24**(11), 2060-2071.
- Shah, S.P., Konsta-Gdoutos, M.S. and Metaxa, Z.S. (2011), *Advanced Cement Based Nanocomposites, Recent Advances in Mechanics*, Springer.
- Sobolev, K. and Gutiérrez, M.F. (2005), “How nanotechnology can change the concrete world”, *Am. Ceram. Soc. Bull.*, **84**(10), 14-18.
- Uddin, S.M., Mahmud, T., Wolf, C., Glanz, C., Kolaric, I. and Volkmer, C. (2010), “Effect of size and shape of metal particles to improve hardness and electrical properties of carbon nanotube reinforced copper and copper alloy composites”, *Compos. Sci. Technol.*, **70**(16), 2253-7.
- Ugheoke, B.I., Onche, E.O., Namessan, O.N. and Asikpo, G.A. (2006), “Property optimization of kaolin-rice husk insulating fire-bricks”, *Leonardo Electronic Journal of Practices and Technologies*, Issue 9, July-December.
- Weitzel, B., Hansen, M.R., Kowald, T.L., Müller, T., Spiess, H.W. and Trettin, H.F.R. (2011), “Influence of multiwalled carbon nanotubes on the microstructure of CSH-phases”, *Proceeding of 13th Congress on the Chemistry of Cement*, Madrid, Spain, July.
- Wenying, G., Guolin, W., Jianda, W., Ziyun, W. and Suhong, Y. (2008), “Preparation and performance of geopolymers”, *J. Wuhan Univ. Tech.-Mater. Sci. Ed.*, **23**(3), 326-330.

- Xie, X., Mai, Y. and Zhou, X. (2005), "Dispersion and alignment of carbon nanotubes in polymer matrix: a review", *Mater. Sci. Eng. R: Report.*, **49**(4), 89-112.
- Yu, X. and Kwon, E. (2009), "A carbon nanotube/cement composite with piezoresistive properties", *Smart Mater. Struct.*, **18**(5), 1-5.

CC